Improvements in seismic event locations in a deep western U.S. coal mine using tomographic velocity models and an evolutionary search algorithm

LURKA Adam[1], SWANSON Peter[2]

[1]*Central Mining Institute, Katowice 40-166, Poland*
[2]*NIOSH/Spokane Research Laboratory, Spokane WA, USA*

Abstract: Methods of improving seismic event locations were investigated as part of a research study aimed at reducing ground control safety hazards. Seismic event waveforms collected with a 23-station three-dimensional sensor array during longwall coal mining provide the data set used in the analyses. A spatially variable seismic velocity model is constructed using seismic event sources in a passive tomographic method. The resulting three-dimensional velocity model is used to relocate seismic event positions. An evolutionary optimization algorithm is implemented and used in both the velocity model development and in seeking improved event location solutions. Results obtained using the different velocity models are compared. The combination of the tomographic velocity model development and evolutionary search algorithm provides improvement to the event locations.

1 Introduction

Developing strategies to deal with ground control hazards requires an accurate picture of the time-dependent, spatially-distributed, deformation processes attending rock mass failures. To the extent that these deformation processes generate detectable seismic emission, location of these events allows these processes to be delineated. Accurate event locations are therefore essential to developing an accurate characterization of critical deformation processes.

The location accuracy of seismic events depends on three main factors: spatial distribution of seismic stations, accuracy of P-wave first-arrival picks and accuracy of the velocity model used in the location algorithm[1–5]. When the geometry of seismic stations is fixed the greatest influence on the location of seismic events is the accuracy of the first arrival picks and accuracy of the velocity model.

P-waves are most often used in event locations because they are easy to identify on seismograms, the picking process is readily automated in software, and the pick errors are generally small. The precision of the first-arrival pick time is limited by the time resolution of the seismic recording equipment. Accuracy of the pick is sensitive to the rate at which the first arriving energy emerges from the background noise. The latter is a function of both source and propagation-path properties. In this regard, possibilities for improvement of pick times are rather limited. Therefore the last factor that can be improved is the velocity model used in the location procedure. This task is especially important when we locate seismic events in mines where the seismic network has a size on the order of a few kilometers and the required location accuracy is a few tens of meters. In seismically active mine areas one observes relatively large variability of P-wave velocity with time thus necessitating periodic updates of the velocity model used in the location process. This article presents an application of velocity images obtained from passive tomography calculations to the problem of seismic event location in a deep western U.S. coal mine.

2 Method

Passive travel-time tomography utilizes seismic events as sources in a simultaneous inversion for event locations and velocity structure. It has been used extensively in studies of earth structure and is being increasingly applied to mining problems[6–9]. The passive tomography problem can be solved in many different ways[6–8,10–11]. Every specific tomography algorithm depends on factors like: the type of

input data, measure of data misfit, minimization method, ray tracing technique, etc.

The present approach to solving passive tomography calculations has been performed using a misfit function based on the L_1 norm. The L_1 norm was selected over the least-squares norm L_2 as it is much less sensitive to the effects of large errors in outlier data[10]. L_1 is given by:

$$L_1(\hat{v},\hat{h}) = \sum_{i=1}^{n}\sum_{j=1}^{m}\left|t_{ij}^{\text{obs}} - t_{ij}^{\text{theor}}\right| \quad (1)$$

where $\hat{v}$ is the vector of velocity model parameters; $\hat{h}$ vector of seismic sources parameters (coordinates and origin times); n number of seismic events; m number of seismic stations; t_{ij}^{obs} observed P-wave travel time; t_{ij}^{theor} P-wave travel time described by model.

The number of variables of the function (1) is a few hundred or more for typical passive tomography problems. To find the minimum of this function we use evolutionary algorithms that are well adapted for optimization problems with a large number of variables. Evolutionary algorithms use the principles of biological progression and try to mimic organic evolution that nature constructed during millions of year[12]. One can assert, in a simplification, that nature acts randomly to some extent but also aims at self perfection. Evolutionary algorithms mimic some of these features in optimization problems.

Evolutionary algorithms have at least three advantages that are especially useful for passive tomography calculations. First, convergence approaches a global minimum. Second, it is easy to apply additional constraints to variables of the optimized function. For example, we can apply additional constraints to velocity values from borehole velocity logs that increase the stability of the algorithm. And third, evolutionary algorithms are adapted to operate on variables that have different physical units, i.e. they are not scaled. In the present application there are variables connected with seismic velocity, seismic event coordinates and event origin times.

A short and very simplified scheme of evolutionary algorithms can be described as follows[12]:

Step 0: Initialization

There should be storage in a digital computer for two points of an n-dimensional Euclidean space

Step 1: Variation

Iteration g. Starting from point $E^{(g)}$ (position signed as a vector $x_E^{(g)}$) a second point $N^{(g)}$ (position signed as a vector $x_{N,i}^{(g)}$) is generated by using random perturbations. This point differs slightly from $E^{(g)}$.

Step 2: Filtration

The two points are associated with different values of the objective function $F(x)$. Only one of them serves as a starting point in the next iteration g+1.

Random perturbations are made by using an n-dimensional Gaussian probability density function with expected values equal to zero and standard deviations equal to σ_i (i=1, 2, ..., n):

$$w(z_1, \ldots, z_n) = \frac{1}{(2\pi)^{n/2}\prod_{i=1}^{n}\sigma_i}\exp\left(-\frac{1}{2}\sum_{i=1}^{n}\left(\frac{z_i}{\sigma_i}\right)^2\right) \quad (2)$$

Graphical illustration of the above steps is shown in Fig. 1.

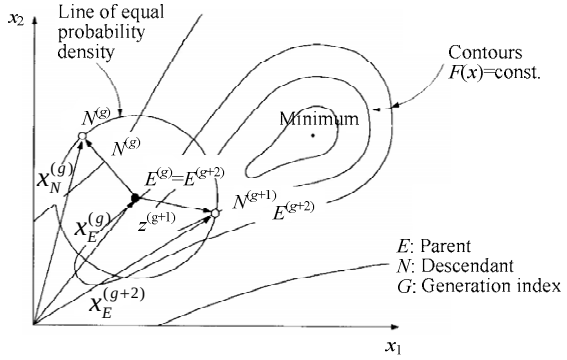

Fig. 1 Schematic illustration of the evolutionary algorithm[12]

Passive tomography calculations, based on evolutionary algorithms and used in this paper, are less time consuming if one assumes that seismic rays are straight lines. This assumption would be a quite good approximation if the velocity contrasts were small and the area of study not large[8].

3 Data

The seismic network consisted of 23 stations equipped with 4.5-Hz geophones. Nine stations were installed on the surface and 14 were installed underground (Table 1). Underground stations were largely located at seam level at a depth of 0.8 km. Both surface and underground seismic arrays operated as separate and independent networks and covered an area measuring 2.3 by 1.5 km. A GPS timing system was used to synchronize both networks, enabling them to operate as one 3-dimensional array. Additional details about the data acquisition and processing system can be found in Swanson[13].

Calculations were performed for seismic events that occurred in the vicinity of an active longwall measuring 250 meters wide by 1500 meters long. About 5000 seismic events were recorded and located using conventional techniques during the study interval. Out of this data set 64 seismograms from well-recorded events with magnitudes M>0.7 were selected for the passive tomography analyses. P-wave first arrivals were manually picked on every seismogram and then the events were located using the layered velocity model given in Table 2. Calculated

event coordinates, origin times and velocity values (Table 2) were used as starting parameters in the passive tomography calculations.

Table 1 Surface and underground seismic stations coordinates

	Station's name	*X* (feet)	*Y* (feet)	*Z* (feet)
Surface	P1G1	81320	17799	7698
	P1G2	82191	17459	8019
	P1G3	82941	17031	7822
	P2G1	82357	15768	8099
	P2G2	83326	15940	7595
	P2G3	83070	14613	7859
	P3G1	81621	18792	7685
	P3G2	82285	19220	7891
	P3G3	83154	18563	7991
Underground	M39L	86329	15024	5860
	M33L	85691	14400	5937
	M26L	84996	13705	6010
	M21L	84518	13205	6062
	M13L	83525	12627	6164
	H21L	84030	16474	5613
	B10L	83350	13829	5992
	B18U	82536	14605	5984
	B26L	81466	15471	5725
	B36L	80504	16519	5588
	B44L	79796	17236	5489
	B62L	79808	18769	5242
	B71L	80647	19700	5120
	TS1L	83802	12898	6125

Table 2 Layered velocity model used in starting location procedure

Elevation (feet)	Velocity (feet/second)
7500~9000	8000
6000~7500	11000
4500~6000	14500

Passive tomography calculations were performed in the area of the active longwall using both surface and underground seismic stations. Calculations were carried out in a 3-layer framework where every layer was subdivided into 8x8 cells. Additional subdivision was applied in the deepest layer where the seismicity was concentrated. The size of this finer scale velocity grid was 12x12 cells. The range of coordinates and the number of cells are shown in Tables 3 and 4.

Table 3 Geometry of velocity grid

	X (feet)	*Y* (feet)	*Z* (feet)
Begining of the grid	79000	12000	4500
End of the grid	87000	20000	9000
Numer of cells	8	8	3

Table 4 Geometry of additional velocity grid in the deepest layer

	X (feet)	*Y* (feet)	*Z* (feet)
Begining of the grid	81000	17000	4500
End of the grid	83000	19000	6000
Numer of cells	12	12	1

4 Results

Fig. 2a shows the seismic ray distribution in the area of interest and Fig. 2b shows the distribution in the region of finer velocity cell subdivision. Fig. 3 illustrates the time residua between measured P-wave first arrivals and theoretical first arrivals for the layered velocity model shown in Table 2 and for the tomographic velocity model (Tables 3 and 4). Fig. 3 allows an assessment of whether the travel time data fit the tomographic velocity model more accurately than the simple layered velocity model. Comparing both histograms of time residua one can see significant improvement between the theoretical and observed first arrivals for the passive tomography velocity model.

Figs. 4a, 4b and 4c show calculated velocity images in the three layers. One can observe horizontal velocity variation in each velocity layer. In the deepest layer (Fig. 4a) P-wave velocity varies from 14000 feet/sec to 14800 feet/sec. In the middle layer (Fig. 4b) velocity varies from 10000 feet/sec to 12000 feet/sec and in the shallowest layer velocity values vary from 7300 feet/sec to 8700 feet/sec. A slightly different velocity image is shown in Fig. 4d for the dense velocity grid in the deepest layer. Horizontal velocity variations are rather minimal and lie between 14460 feet/sec and 14510 feet/sec in the larger part of the region.

The calculated velocity model presented in Fig. 4 has been used to relocate seismic tremors with magnitude $M \geq 0.7$. Fig. 5 shows, in the planes *XY* and *XZ*, seismic tremors located by using both the velocity model from Table 3 and the velocity model determined in the tomographic inversion. The spatial differences in the event locations reach values exceeding 200 feet (about 60 meters). Therefore, it is clearly seen that the tomographic velocity model fits the arrival-time data better and the relocation using the tomographic velocity model differs substantially from the locations using the layered constant velocity model.

However, the relocation of seismic tremors did encounter some difficulties due to the existence of many minima in the solution procedure. In such cases the location process was repeated many times using different starting points and the position with the smallest value of the misfit function was assigned to be the event location. The occurrence of many minima in the misfit function was caused probably by applying tomographic velocity model that is strongly heterogeneous.

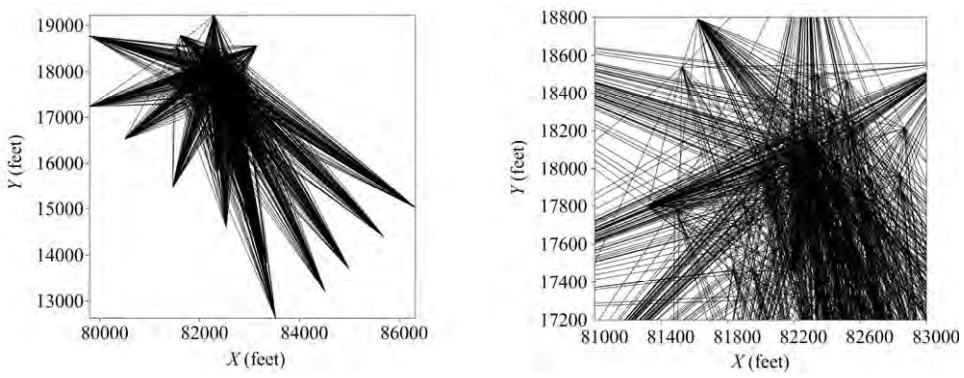

(a) Region including all seismic stations (b) Area with finer velocity grid

Fig. 2 Ray path coverage for seismic events with magnitude $M \geq 0.7$

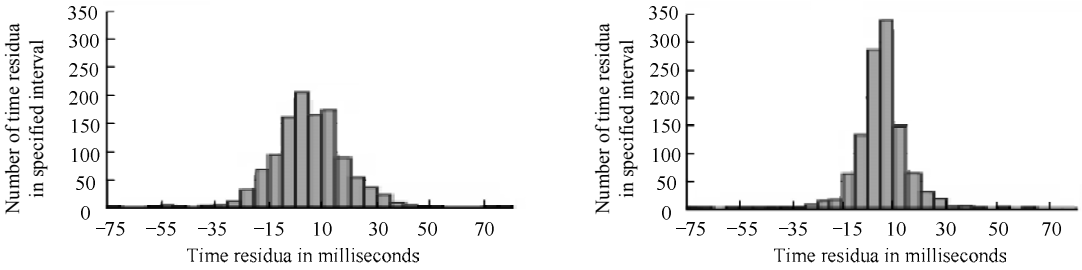

(a) 3-layer constant-velocity model (b) Tomographic velocity model

Fig. 3 Time residua for the 3-layer constant-velocity model and for tomographic velocity model

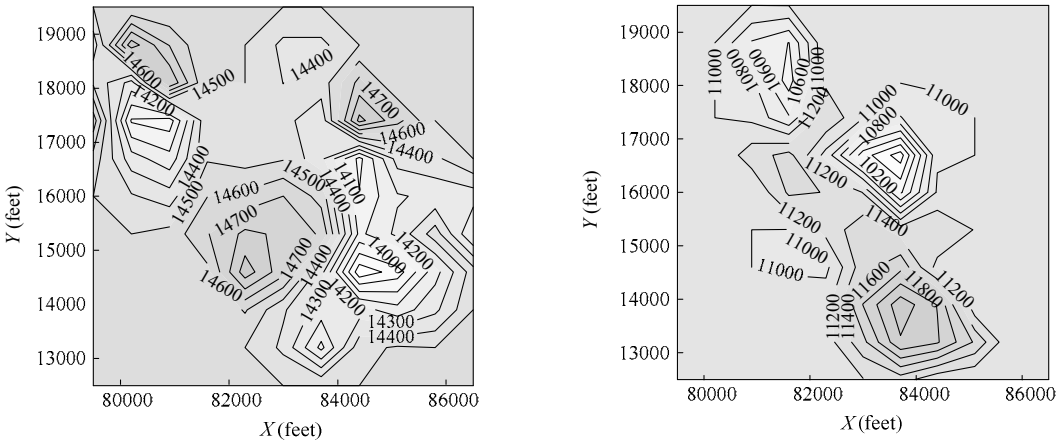

(a) The deepest layer: from Z=4500 to Z=6000 feet (b) The middle layer: from Z=6000 to Z=7500 feet

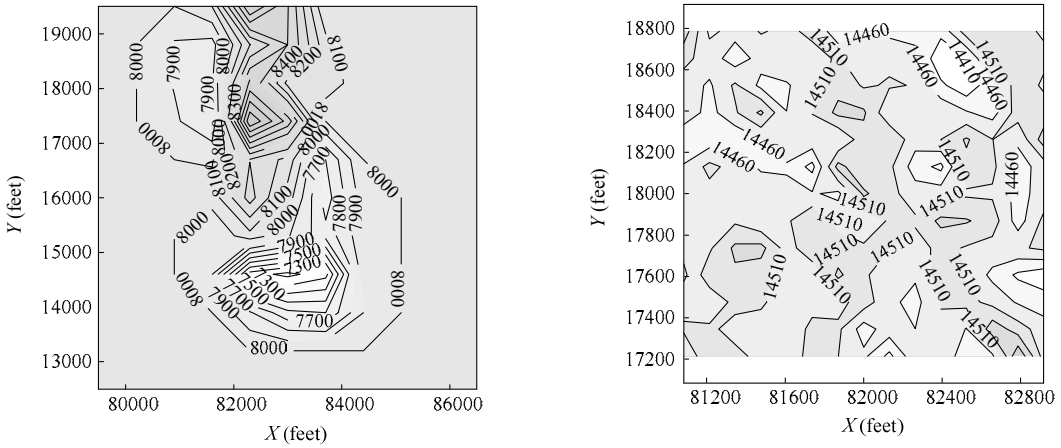

(c) The surface layer: from Z=7500 to Z=9000 feet (d) Area with increased density of grid cells

Fig. 4 Map showing velocity model (feet/sec) obtained from passive tomography calculations

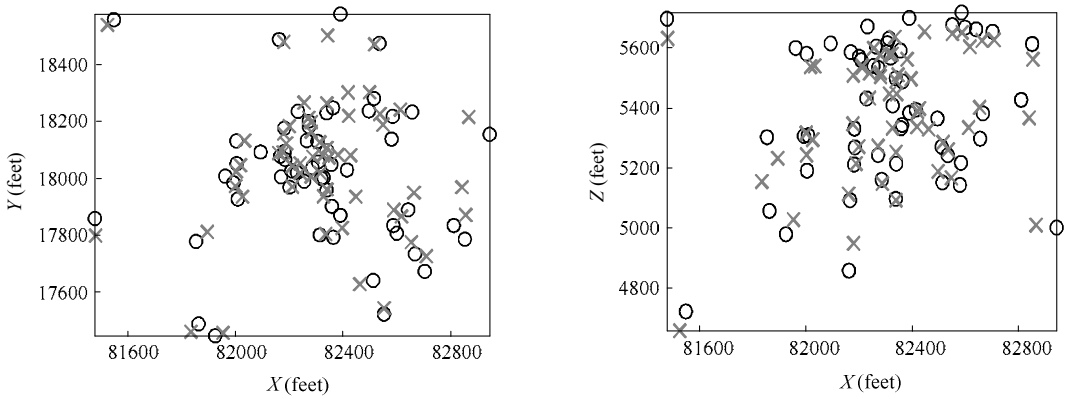

(a) Horizontal plane *XY* (b) Vertical plane *Z*

Fig. 5 Horizontal plane *XY* and vertical plane *Z*

(Cross symbols show positions of seismic events calculated by using 3 layer constant velocity model; circle symbols show positions of seismic events calculated by using tomographic velocity model)

5 Conclusions

Methods to improve seismic tremor location accuracy in a deep western U.S. longwall coal mine by using tomographic velocity images have been considered. Tomographic velocity model and event location calculations have been carried out using arrival-time data from digital seismograms of mining-related seismic activity recorded by a local seismic network. Velocity images have been obtained using a passive tomography method. The calculated tomographic velocity model has been used to relocate seismic events. Passive tomography calculations have been carried out by using evolutionary algorithms that are well-suited to seeking the global minimum of the multidimensional functions.

Differences between locations of seismic tremors obtained by using constant layered and tomographic velocity models were on the order of a few tens of meters. It follows that the tomographic P-wave velocity model has a significant impact on the seismic tremor locations. As the three-dimensional velocity model fits the theoretical P-wave travel times better than the constant velocity layered model one can say that this location procedure improves the event location accuracy. Additionally, in seismically active mines where one observes changes of velocity in time due to mining, periodic calculations of the velocity structure should be conducted using such passive tomographic methods.

During relocations of seismic events using the tomographic velocity model one can observe unfavorable phenomenon associated with a relatively large number of local minima in the misfit function. It is likely caused by using complicated heterogeneous velocity model in the location algorithm.

This paper was partially supported by the advanced NATO fellowship program.

References

[1] Rabinowitz N, Steinberg D M. Optimal configuration of seismographic network: a statistical approach. *Bull Seism Soc Am*, 1990.

[2] Swanson P, Estey L, Boler F, Billington S. Mining-induced microseismic event location errors: accuracy and precision of analog and digital systems. *Pure and Appl Geophys*, 1992(139): 375–404.

[3] Mendecki A J. *Seismic Monitoring in Mines*. Cambridge: Chapman & Hall, 1997.

[4] Dubiński J, Drzęźla B. Location of seismic events in mines. *In: Biblioteka Szkoly Eksploatacji Podziemnej*. Kraków, 1995. (In Polish)

[5] Gibowicz J G, Kijko A. *An Introduction to Mining Seismology*. London: Academic Press, 1994.

[6] Iyer H M, Hirahara K. Seismic tomography. *Theory and Practice*. London: Chapman & Hall, 1993.

[7] Maxwell S C, Young R P. A comparison between controlled source and passive source seismic velocity images. *Bull Seism Soc Am*, 1993, 83(6): 1813–1834.

[8] Maxwell S C, Young R P. Seismic velocity inversion from microseismic data. *Seismic Monitoring in Mines*. London: Chapman & Hall, 1997.

[9] Lurka A. Seismic hazard assessment in the Bielszowice coal mine using passive tomography. *Seismogenic Process Monitoring*. Tucson: A. A. Balkema Publisher, 2002.

[10] Tarantola A. *Inverse Problem Theory*. Amsterdam: Elsevier, 1986.

[11] Shalev E, Lees M. Cubic B-splines tomography at loma prieta. *Bull Seism Soc Am*, 1998, 88(1): 256–269.

[12] Schwefel H P. *Evolution and Optimum Seeking*. London: John Wiley & Sons, 1995.

[13] Swanson P. Development of an automated pc-network-based seismic monitoring system in dynamic rock mass response to mining. *In: Proceedings of the 5th International Symposium on Rockbursts and Seismicity in Mines*. Johannesburg, 2001: 11–17.